JOURNAL OF SPACECRAFT AND ROCKETS
Vol. 33, No. 3, May–June 1996

Hypersonic Nozzle–Afterbody Experiment: Flow Visualization and Boundary-Layer Measurements

Earl R. Keener*
Eloret Institute, Palo Alto, California 94303
and
Frank W. Spaid†
McDonnell Douglas Corporation, St. Louis, Missouri 63166

This study was conducted to characterize experimentally the flowfield created by the interaction of a single-expansion-ramp nozzle flow with a hypersonic external stream. Data were obtained from a generic nozzle–afterbody model in the 3.5-Ft Hypersonic Wind Tunnel of the NASA Ames Research Center in a cooperative experimental program involving NASA Ames and McDonnell Douglas Corporation. The model design and test planning were performed in close cooperation with members of the Ames computational fluid dynamics (CFD) team for the National Aero-Space Plane Program. Experimental results are presented, consisting of oil-flow and shadowgraph flow-visualization photographs, afterbody surface-pressure distributions, forebody and nozzle boundary-layer rake measurements, and Preston-tube skin-friction measurements. The oil flows show the outward turning of the underexpanded jet at the cowl exit, and the interaction of a jet-plume internal shock with the nozzle boundary layer. Shadowgraph photographs show the forebody boundary layer, shock waves in the external flow and the jet, and the shear layer between the jet and the external flow. These data are available for CFD code validation.

Nomenclature

C_f = local skin-friction coefficient, τ_w/q_e
d = Preston-tube diameter
H = boundary-layer shape factor, δ^*/θ
M = Mach number
n = boundary-layer velocity profile exponent
p = pressure
q = dynamic pressure, $\frac{1}{2}\rho u^2$
Re = unit Reynolds number
Re_θ = Reynolds number based on momentum thickness
u = velocity
u_τ = shear velocity, $(\tau_w/\rho_w)^{1/2}$
x = streamwise distance from combustor exit station, positive downstream
y = spanwise distance, positive to right when facing in positive x direction, origin at center of combustor exit station at inner surface of cowl
z = vertical distance, normal to $x-y$ plane, positive downward
δ = boundary-layer thickness
δ^* = boundary-layer displacement thickness, $\int_0^\delta [1-(\rho u/\rho_e u_e)]\,dz$
θ = boundary-layer momentum thickness, $\int_0^\delta \{(\rho u/\rho_e u_e)[1-(u/u_e)]\}\,dz$
ν = kinematic viscosity
ρ = density
τ = shear stress

Subscripts

e = conditions at edge of boundary layer
j = jet flow conditions
t = total conditions
w = conditions at the wall
∞ = freestream conditions

Received April 22, 1994; revision received July 6, 1995; accepted for publication July 6, 1995.

*Research Scientist, NASA Ames Research Center, MS 203-2, Moffett Field, CA 94035-1000. Associate Fellow AIAA.
†Group Manager, Experimental Fluid Dynamics, Advanced Flight Technology. Associate Fellow AIAA.

Introduction

THE National Aero-Space Plane (NASP) was intended to rely on an airbreathing propulsion system based on scramjet engine technology during a major portion of its mission. To contribute to the NASP research effort, NASA Ames Research Center conducted a comprehensive experimental and computational investigation of selected generic components of the NASP configuration. An important aspect of the NASP technology development is the propulsion-system–airframe integration. Accordingly, the NASA Ames 3.5-Ft Hypersonic Wind Tunnel was used to conduct a series of tests on a generic nozzle–afterbody configuration.

Many difficulties associated with the development of a hypersonic vehicle arise from the fact that major portions of the flight environment cannot be simulated by existing ground-test facilities. Therefore, numerical simulations of aerodynamic and propulsion flowfields obtained from computational fluid dynamics (CFD) codes will be used extensively to complement data obtained from experimental facilities. Confidence in predictions of the codes can be developed only by making detailed computational–experimental comparisons at conditions for which experimental data are available.

A roadmap of CFD validation experiments for hypersonic flows was presented by Marvin.[1] The present experiment is listed as a recommended nozzle benchmark validation experiment in Ref. 1. The purpose of this experiment is to experimentally characterize the flowfield created by the interaction of the plume from a single-expansion-ramp nozzle (SERN) with a hypersonic external flow. All aspects of the test were planned with a view toward facilitating comparisons of the data with CFD predictions.

Important aspects of jet-plume–external-flow interactions are present in this experiment. Departures from simulation requirements for the flight environment were necessitated by the nature of the facility and by the available resources, and are justified because the primary test objective is to obtain data for CFD code validation. A more complete discussion of simulation requirements is given in Ref. 2.

This paper is the first in a two-part series and includes experimental results consisting of oil-flow and shadowgraph flow-visualization photographs, afterbody surface-pressure distributions, boundary-layer rake measurements, and Preston-tube skin-friction measurements. The second part[3] presents results of five-hole- and thermocouple-probe surveys. Portions of these data and preliminary comparisons of experiment and results of CFD computations have been previously reported.[4–7]

Experimental Methods

Facility

The NASA Ames 3.5-Ft Hypersonic Wind Tunnel is a closed-circuit, blowdown wind tunnel and has interchangeable, contoured, axisymmetric nozzles. The test gas is heated air. During this experiment the tunnel was operated with the Mach 7.3 nozzle for runs of approximately 2-min duration.

SERN Model

The primary features of the generic SERN model design are shown in a schematic diagram (Fig. 1) and a photograph (Fig. 2). The objective of the design was to provide a wind-tunnel model that would create a large-scale nozzle-jet-plume flow over a representative afterbody. CFD computations played a major role in the model design process.[4] Except for the cowl, the side view of the model is a parallelogram. The forebody is a wedge whose upper surface is a flat plate with a nominally sharp leading edge (0.12-mm thickness). A removable boundary-layer trip is provided for the upper surface at a short distance downstream of the leading edge. The design and location of the trips are based on experimental data reported by Hopkins et al.[8] and Keener and Hopkins.[9] The model is supported from below on a swept strut with a wedge-shaped leading edge. After the tunnel free-jet flow is established, the model-support system translates to insert the model into the flow.

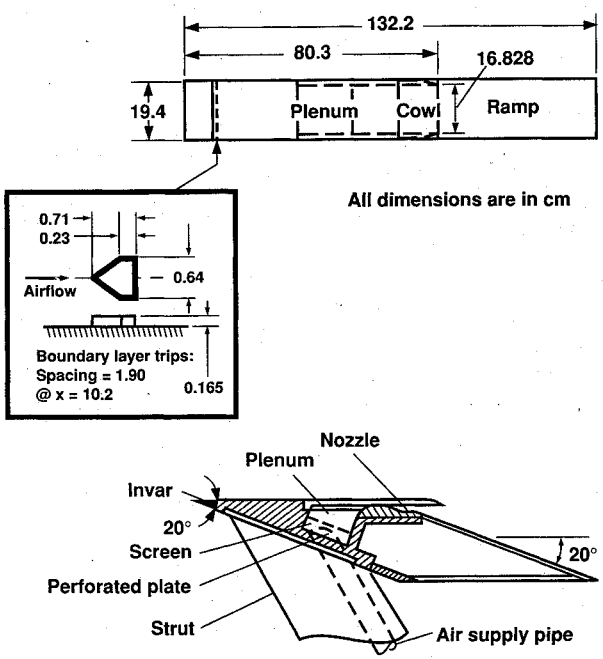

Fig. 1 Schematic of hypersonic SERN model.

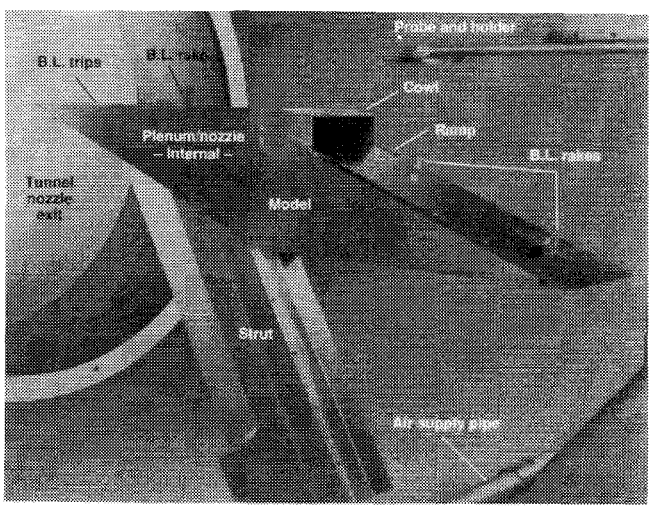

Fig. 2 Photograph of hypersonic SERN model installed in NASA Ames 3.5-Ft Hypersonic Wind Tunnel.

Air is supplied to a plenum through a supply pipe in the model-support strut. A perforated plane and two screens condition the flow within the plenum. The internal surface of the cowl is flat, and a nozzle block is mounted in the model between the plenum and the ramp. The internal nozzle exit is intended to simulate a combustor exit station. The nozzles were designed by the method of characteristics, with a boundary-layer correction, to provide uniform flow at the combustor-exit station. For this test, the nozzle was designed for a combustor-exit Mach number of 1.75. The external cowl surfaces are curved, resulting in a 1.5-mm cowl trailing-edge thickness. Additional details of the model design are presented in Refs. 2 and 6.

The air supply to the nozzle is obtained from the NASA Ames 3000-psi air supply system through a system of valves and regulators. The system allows a predetermined jet plenum pressure to be rapidly established and maintained at a constant value.

Instrumentation and Measurements

The jet total pressure and temperature were measured with two pitot tubes and a thermocouple in the plenum chamber downstream of the screens. The jet mass flow rate was measured with an ASME orifice meter[10] in the air supply pipe upstream of the model. These measurements were in good agreement with computations of the mass flow rate using the jet plenum conditions and the nozzle throat area corrected for boundary-layer displacement.

Two ramp plates were tested downstream of the combustor exit station. A noninstrumented ramp plate was used for oil-flow visualization photographs; shadowgraph photographs were obtained with both ramps. One ramp plate was extensively instrumented with static-pressure orifices. The locations of the orifices on the ramp and on the forebody of the model are shown in a plan view in Fig. 3. The pressures are measured by arrays of electronically scanned solid-state transducers installed within the model. Boundary-layer measurements were made with three small, fixed pitot-pressure rakes on the ramp and forebody (Figs. 2 and 3). Skin friction was measured with three Preston tubes. Pitot-pressure surveys were made at the combustor exit with the cowl off and no tunnel flow to assure that the flow was uniform at this station.

Corrections for calorically-imperfect-gas effects were included in the data reduction equations. Wind-tunnel freestream conditions were calculated from the measured reservoir total pressure and temperature and from pressures measured by two pitot tubes mounted near the leading edge of the model.

Accuracy

The estimated probable uncertainties of pertinent recorded and calculated quantities are as follows: M_∞, $T_{t\infty}$, T_{tj}, and $p_{t\infty}$, ±2%; Re/m, ±8%. These values are derived from tunnel calibration data and from analysis of calibration procedures and data repeatability from the present investigation.

Test Conditions

For the majority of runs, the model was mounted with its leading edge 3.8 cm downstream of the tunnel nozzle exit. The forebody top surface was set at an angle of −1.1 deg (compression) with respect to the tunnel centerline. The model was set at this negative angle to increase the forebody top-surface pressure somewhat so as to

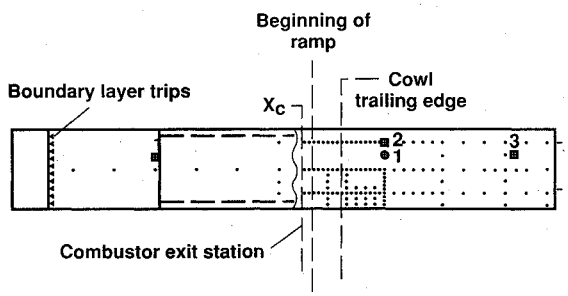

Fig. 3 Plan view of model instrumentation locations: ·, surface pressure orifices; ⊞, boundary layer rakes (3); and ⊕, preston tubes (3).

counter the tendency of the top-surface flow on the wedge-shaped forebody to flow inward.[8,9]

The baseline test conditions established for this experiment are summarized in Table 1, which includes nominal values, variations among runs, and variations within runs. The axial Mach-number gradient was obtained from tunnel calibration data and verified by data obtained from the model pitot tubes. The combustor exit Mach number and pressure ratio are representative of scramjet operation at the indicated value of freestream Mach number. The jet was underexpanded at the cowl exit at the baseline jet pressure ratio. Ramp pressure data were obtained at other pressure ratios and also at one-half the baseline freestream total pressure.

Local Mach number on the forebody top surface was calculated from the freestream Mach number, the tunnel total pressure, and the average of the forebody static pressures. The resulting value was 7.11, which is in good agreement with the computed value corresponding to a 1.1-deg compression at the freestream Mach number.

Results and Discussion

Oil-Flow Visualization

Baseline Test Condition

Figure 4a shows results of an oil-flow test on the model cowl and ramp at the baseline test conditions. The oil-flow streaks ahead of the cowl show that the flow into the jet is streamwise at the model test angle of −1.1 deg. A transverse separation line (oil-accumulation line) is present on the upper surface of the cowl ahead of the trailing edge. This feature is consistent with the evidence of separation on the cowl from the shadowgraphs. The flow separation was expected because of the combination of curvature in the design of the cowl exterior and the compression corner produced by the underexpanded jet.

Table 1 Baseline test conditions and variations

Quantity	Nominal value	Variation among runs	Variation during a run
M_∞	7.33	±0.025%	——
dM_∞/dx	0.177/m	——	——
$p_{t\infty}$	6,895 kPa	±0.2%	±0.1%
$T_{t\infty}$	828 K	±5.8%	±1%
Re_∞	14×10^6/m	——	——
p_{tj}	374 kPa	±3%	±1%
T_{tj}	272 K	±2%	±2%
p_{tj}/p_∞	310	±3%	±1%
M_j	1.74	±0.005	±0.005

The oil-flow pattern inside the cowl (not shown) was two-dimensional with no separation at the corners. The oil-flow pattern on the ramp is symmetrical, with the centerline flow straight down the ramp. The surface flow direction turns outboard at the cowl trailing edge on each side. This outboard turning is a result of the lateral jet-flow expansion from the vertical cowl side trailing edge. The onset of outboard turning approaches the centerline with increasing distance down the ramp.

A symmetric pair of separation lines first occurs on each side of the ramp, slightly outboard of the cowl exit, and curves inboard, almost intersecting at the center of the ramp trailing edge. These are believed to be associated with the interaction of a shock wave, called the jet-plume internal shock wave (see the discussion of shadowgraph flow visualization), with the ramp boundary layer. The trajectory of this shock wave is undoubtedly influenced by the proximity of the model side edge. Outboard of these separation lines, the oil streaks flow inboard, indicating a vortical flow around the ramp side edge.

Figure 4b shows an enlargement of the oil-flow photograph for the ramp from Fig. 4a with contour lines of constant flow angle superimposed. The outward turning angles increase to more than 20 deg. The line for zero angle starts from the cowl trailing edge and sweeps inboard to the ramp centerline. This swept zero-angle line is related to the first wave line of expansion of the lateral flow from the vertical trailing edge at the side of the cowl. Over the rearward two-thirds of the ramp, the zero-angle line is the ramp centerline. The flow angle increases with increasing spanwise and chordwise distance.

Figure 4c shows the oil-flow pattern on the side of the model. The oil streaks show that the flow around the lower model corner from the high-pressure region on the lower surface to the lower-pressure regions on the side is nearly streamwise on the top half of the model. Disturbances on the lower half of the model are associated with the

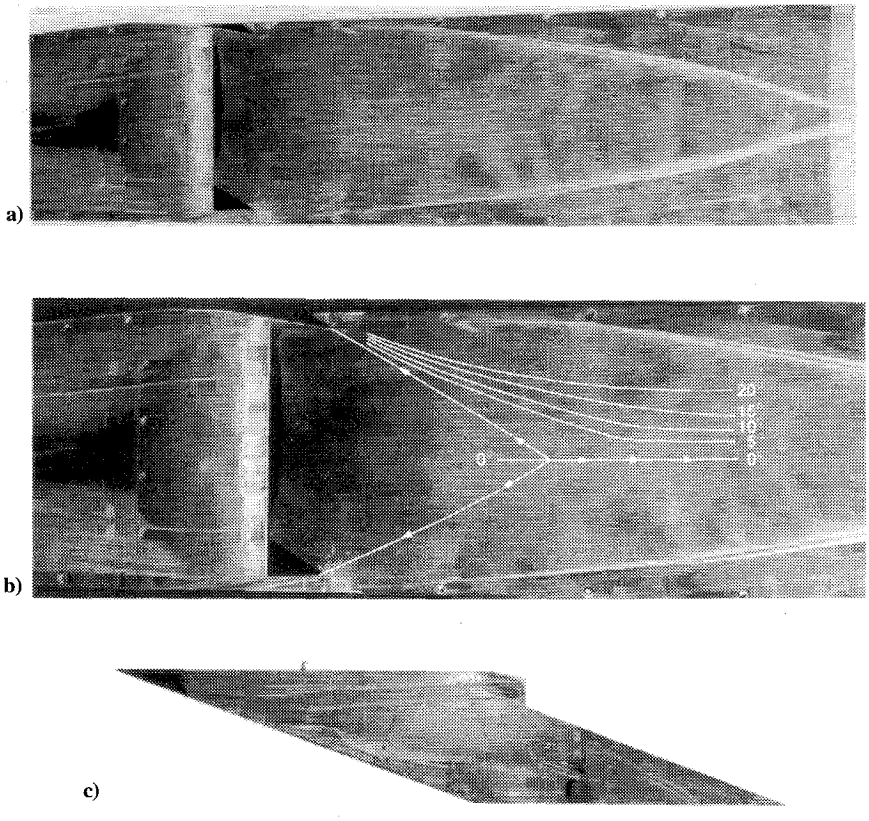

Fig. 4 Oil-flow photographs at baseline test condition, p_{tj}/p_∞ = 310: a) top view, b) ramp surface flow angles, and c) side view.

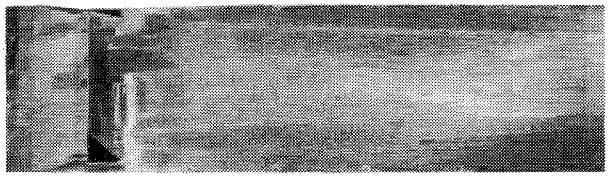

a) $p_{tj}/p_\infty = 154$

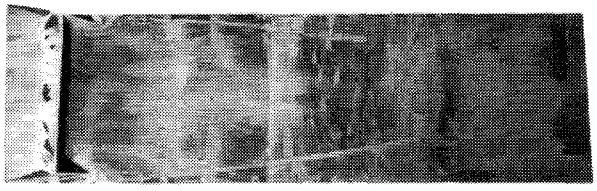

b) $p_{tj}/p_\infty = 234$

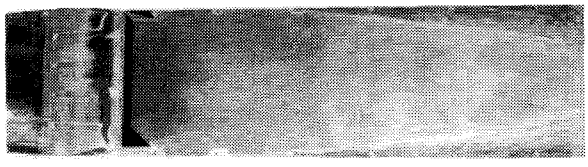

c) $p_{tj}/p_\infty = 620$

Fig. 5 Oil-flow photographs of ramp at off-design conditions.

strut and do not appear to influence the ramp and jet flowfield. A feature that appears to be a separation line originates at the jet exit and reaches the lower corner of the model upstream of the ramp trailing edge. This line is believed to be associated with the external jet-plume shock wave (seen in the shadowgraphs) that wraps around to the side of the model.

Effects of Jet-Pressure Ratio

Figures 5 presents the results of oil-flow tests at off-design jet-pressure ratios of $p_{tj}/p_\infty = 154, 234$, and 620 (recall that the baseline value is 310). Figure 5a shows the results of an oil-flow test at a jet-pressure ratio of $p_{tj}/p_\infty = 154$ at $p_{t\infty} = 6895$ kPa and $p_{tj} = 186$ kPa. The oil-flow pattern shows that the jet is not flowing full from the cowl. It appears that the jet is separating in the cowl–ramp side corners. These flow disturbances are asymmetric and probably unsteady. The separated flow attaches on the ramp behind the heavy oil line and flows nearly straight to the ramp trailing edge. The extent of separation near the trailing edge of the cowl is shorter because of the reduced jet total pressure. Figure 5b shows the results of an oil-flow test at a jet-pressure ratio of $p_{tj}/p_\infty = 234$ at $p_{t\infty} = 6895$ kPa and $p_{tj} = 283$ kPa. This pattern was obtained by applying two lateral and several vertical bands of oil. In Fig. 5b the oil flow over the rear half of the ramp is not of good quality; however, near the cowl the oil-flow quality is sufficient to determine that the flow is attached. (The smeared oil in the lower corner of the cowl is not part of the oil-flow pattern.) The upper corner shows smooth, attached flow. Figure 5c shows the results of an oil-flow test at an increase in jet-pressure ratio to $p_{tj}/p_\infty = 620$ at $p_{t\infty} = 3447$ kPa and $p_{tj} = 374$ kPa. This test was made to determine whether the large increase in jet-pressure ratio would significantly affect the jet separation pattern on the ramp, perhaps moving the separation lines closer to the edges of the model. The photograph shows that the increase in jet-pressure ratio moved the separation lines out to the model edges on the forward part of the ramp, changing to about half way to the edges on the rearward part. The streamwise separation distance near the trailing edge of the cowl increased because of the increased outward flow-deflection angle at the higher pressure ratio.

Shadowgraph Flow Visualization

Forebody

Figure 6a is a shadowgraph of the flowfield over the forward part of the model, and Fig. 6b shows the remainder of the forebody flowfield, followed by the jet plume. Both photographs were obtained at the baseline test conditions.

Figure 6a shows that the forebody shock wave is weak above the top surface. Weak shock waves occur off the boundary-layer trips. Results of a previous investigation[9] showed that identical trips did not adversely affect the downstream boundary-layer characteristics at the same value of the local Reynolds number, but caused earlier transition. The boundary-layer trips were required because even the small bluntness of the present model causes a profound increase in the length of laminar flow.[8,9] The boundary layer on the top of the forebody is prominent in the shadowgraphs. The boundary layer and its edge look smooth directly behind the trips, but between the trips and the boundary-layer rake the boundary layer becomes turbulent. The complete transition process at Mach 7.3 takes place over an appreciable length that is almost equal to the length at the onset. The appearance of transition onset in Fig. 6a is well forward of the cowl trailing edge. The boundary-layer thickness, as it appear in the shadowgraph, grows to over 1.25 cm at the beginning of the cowl curvature.

The shadowgraph photograph of Fig. 6b shows the remainder of the flowfield ahead of the jet plume. The shock wave that exists at the edge of the tunnel free-jet flow is seen near the top of the shadowgraph. The tunnel jet flow expands slightly at Mach 7.3, and this shock wave exists where the outer part of the jet flow turns back slightly. A CFD-code study of this tunnel-jet expansion, resulting in a small axial-Mach-number gradient, concluded that its effect on the jet plume is negligible.[5] The forebody boundary layer thickens on the curved portion of the cowl and separates ahead of the cowl trailing edge because of the compression caused by the plume shock and the external curvature of the cowl. The boundary layer passes through the jet-plume shock wave into the jet-plume shear layer.

Jet Plume

The shadowgraph in Fig. 6b shows the jet plume and the interaction of the underexpanded jet with the external flow. The jet-plume external shock wave is caused by the outward turning of the underexpanded jet flow. Underneath the jet-plume shock wave is the shear layer between the jet and the external flow. The shear layer begins at the cowl trailing edge as a thin, sharply defined layer that rapidly increases in thickness and appears to be highly turbulent. The forebody boundary layer appears to merge with the shear layer above the cowl trailing edge and the separated-flow region. The forebody boundary layer probably has a significant effect on the subsequent development of the shear layer, and should be considered in attempts to compute this flowfield.

An internal shock wave in the jet originates near the cowl trailing edge. This shock wave is believed to be analogous to the so-called barrel shock observed in underexpanded jets exhausting into a quiescent medium, and is also observed in jet- and rocket-exhaust flows. The dark area near the cowl lip is possibly a region of high pressure and density gradients caused by the expansion of the jet as it leaves the cowl. Under the expansion region emanating from the cowl trailing edge, there is a white line that also emanates from the cowl trailing edge and extends almost parallel to the ramp back to the boundary-layer rake. Apparently this line is the boundary between the expansion region influenced by waves originating from the cowl trailing edge and the expansion region emanating from the 20-deg radius, which provides a transition from the internal nozzle to the ramp. Between the white line and the ramp lies the expansion field that emanates from the nozzle-to-ramp transition surface. There are also several weak shock waves in this region, radiating from inside the cowl from the beginning of the ramp. Most of these waves emanate from disturbances at the junction between the ramp and the nozzle block.

Shadowgraph photographs illustrating the effects of variations in jet-pressure ratio are presented in Refs. 2 and 6. The internal shock wave, shear layer, and external shock wave are closest to the ramp in the immediate vicinity of the cowl trailing edge at the intermediate jet-pressure ratio of $p_{tj}/p_\infty = 158$, and move away from the ramp as the pressure ratio increases or decreases above or below this value. The oil-flow photographs explain this behavior. At lower jet-pressure ratios, the nozzle flow is not full, and flow

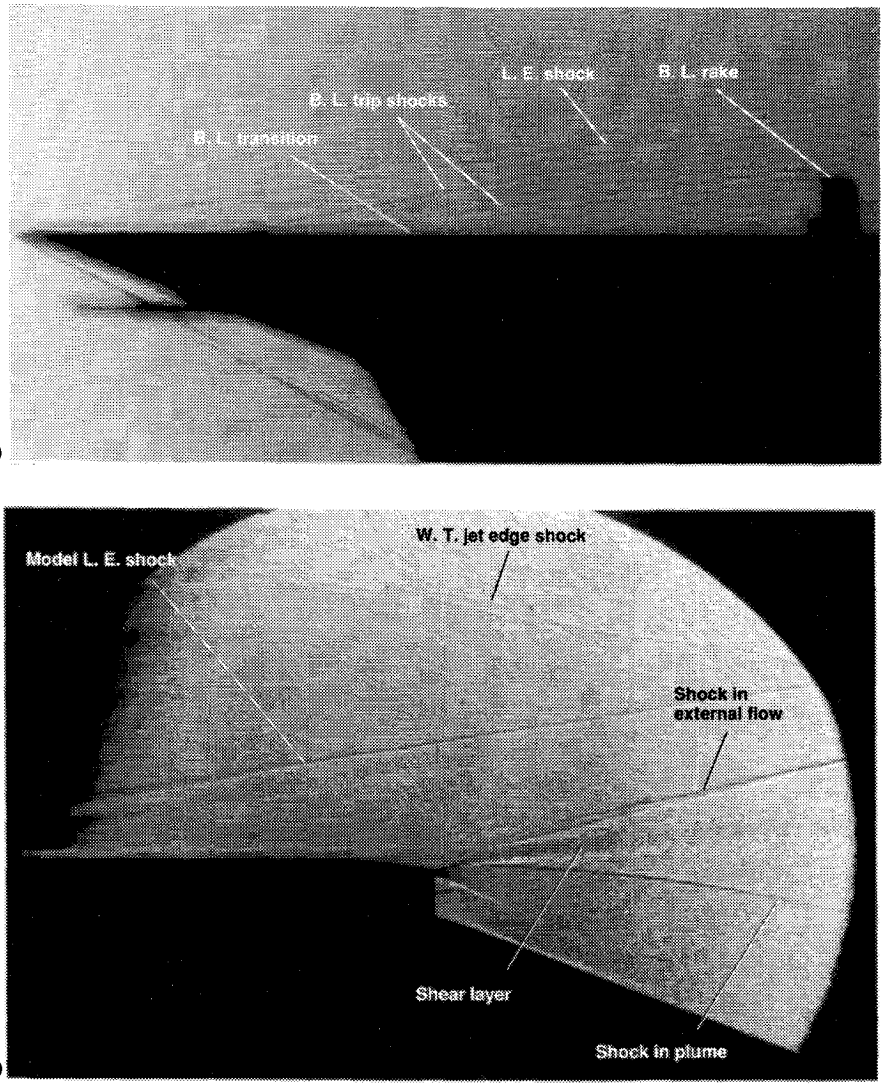

Fig. 6 Shadowgraph photographs at baseline test condition, p_{tj}/p_∞ = 310: a) forebody and b) jet plume.

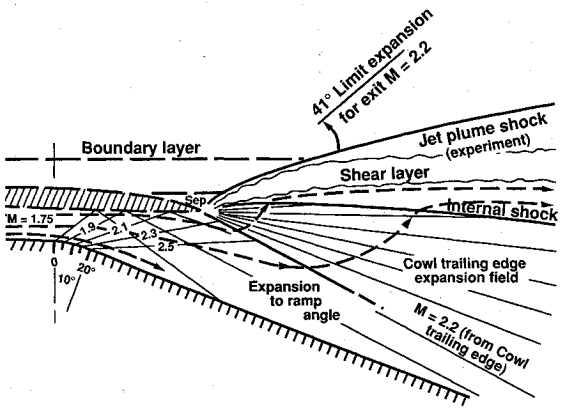

Fig. 7 Schematic of vertical cross section and wave diagram of internal nozzle, cowl, and jet plume at baseline test conditions.

separation occurs on the ramp at the cowl, decreasing the effective cross-sectional area at the cowl. At the higher pressure ratio, the shocks and shear layer are forced outward.

Sketches of the Jet–External-Flow Interaction

Figure 7 shows a vertical cross section of the model and jet plume at the plane of symmetry, including a sketch of the nozzle internal contour. Lines representing expansion waves emanate from the 20-deg radius beginning at the internal nozzle exit (combustor exit station). The first three wave lines in the sketch intersect the inside of the cowl, while downstream wave lines exit the cowl and interact with the expansion field beginning at the cowl trailing edge and the shear layer.

The white line in shadowgraph photographs beginning at the cowl trailing edge and extending almost parallel to the ramp is believed to be the first expansion wave from the cowl trailing edge. This conclusion is substantiated by the change in slope of a pitch-plane flow-angle distribution obtained from a five-hole probe survey 4.6 cm downstream of the cowl.[2,6] The initial change in slope of the pitch-plane angle distribution within the jet flow occurs at z = 2.4 cm, which is in good agreement with the location of the white line at this streamwise station from the shadowgraph photograph of Fig. 6, and is also in good agreement with the location of the intersection of a Mach wave corresponding to Mach 2.2 extended from the cowl trailing edge. The interaction of the expansion waves from both the nozzle-to-ramp transition surface and the cowl trailing edge causes them to bend away from the jet-flow primary direction. The interaction of the expansion waves from the transition surface with the shear layer causes the shear layer to bend toward the ramp.

The extent of the region where the flow over the ramp is independent of the details of the interaction with the external flow is determined by the distance required for expansion waves from the cowl trailing edge to reach the ramp. The white line conservatively represents the boundary of the region of isolation, although the isolated region also includes the region of expansion of the flow from the cowl trailing edge before the expansion waves reflect back to the

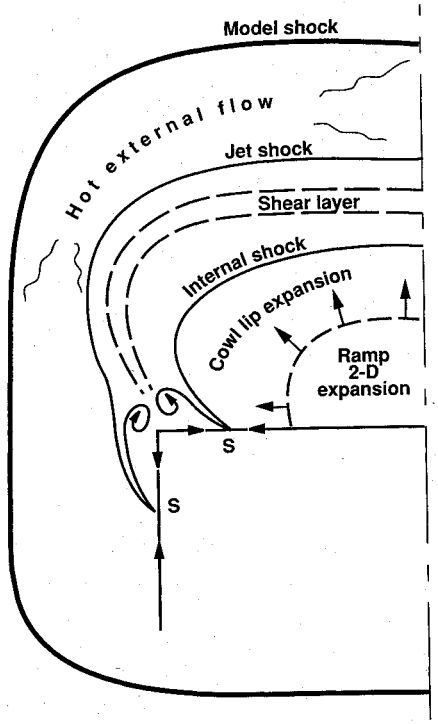

Fig. 8 Schematic of a transverse cross section of jet plume.

ramp. Thus, much of the forward ramp surface flow is independent of the flow characteristics at the edge of the jet.

The remainder of the sketch depicts the shadowgraph results: inner and outer shock waves, jet shear layer, forebody boundary layer, and separation near the cowl trailing edge. Flow streamlines are also shown, which depict the inner flow turning down the ramp, the outer flow turning outward, and the slight turning back through the inner shock wave.

A sketch of a horizontal cross-sectional view through the jet is presented in Refs. 2 and 6. The primary features of the flow in this plane are similar to those presented in Fig. 7, except that there are no waves analogous to those caused by the ramp expansion. The flow is streamwise from the cowl until it encounters the lateral expansion waves from the cowl vertical trailing edge and turns outward. Looking at the oil-flow-angle sketch in Fig. 4b, we see that the contour where the flow begins to turn outward (the zero-angle line) must be the beginning of the expansion region from the cowl trailing edge. Within this boundary is a conical-shaped region where the flow is expanding two-dimensionally as a result of the 20-deg turning angle for the ramp.

Figure 8 is a sketch of a transverse cross section near the cowl where two-dimensional ramp flow exists over part of the ramp span, outboard of which the flow turns outward. There is a boundary line separating the inner region of two-dimensional expanding flow originating at the curved transition downstream of the nozzle exit and the outer region of three-dimensional expanding flow originating at the cowl trailing edge. Downstream of the conical line for zero flow angle (Fig. 4b), the flow expands three-dimensionally outward from the center of the jet plume. The jet does not expand smoothly to the side edge of the ramp, but separates (S) because of the influences of the model side edge and the internal shock within the jet. The shear layer extends above and outboard of the cowl platform, but it is likely that the shear layer merges with the corner flow. The inner shock wave lies inside the shear layer and probably induces the jet-flow separation on the ramp. The outer shock wave surrounds the jet plume, which expands upward and outward from the cowl trailing edge, and ends at the model side where the oil-flow separation line appears.

Boundary-Layer Rake Data

A summary of boundary-layer rake data is given in Table 2. Mach numbers were computed from rake pitot pressures and the local surface pressures by using the Rayleigh pitot formula with corrections

Table 2 Boundary-layer rake data summary[a]

Position	p_{tj}/p_∞	δ^*	θ	Re_θ	H	C_f
No. 1—forebody rake:	——	0.367	0.0236	3740	15.53	0.00127
$x = -36.5$	——	0.335	0.0244	3533	13.71	0.00130
$y = -3.96$						
No. 2—forward ramp rake:	312	0.178	0.0272	6230	6.53	0.00193
$x = 19.84$	197	0.181	0.0278	3853	6.49	0.00204
$y = -6.086$	118	0.188	0.0282	2278	6.66	0.00248
	316	0.152	0.0233	5181	6.53	0.00202
	307	0.164	0.0249	5462	6.58	0.00201
No. 3—aft ramp rake:	312	0.343	0.0366	2470	9.40	0.00221
$x = 49.58$	197	0.436	0.0545	2296	7.99	——
$y = -2.86$	316	0.342	0.0378	1954	9.06	0.00241
	307	0.375	0.0400	1575	9.38	0.00227

[a]Baseline test conditions: nominal $p_{t\infty} = 6895$ kPa, nominal $T_{t\infty} = 828$ K. Dimensions in centimeters.

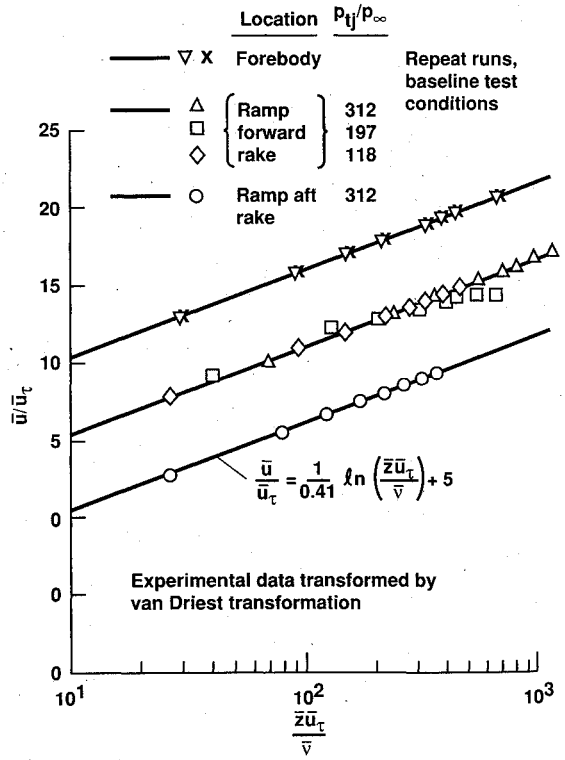

Fig. 9 Forebody and ramp boundary-layer rake data in law-of-the-wall coordinates.

for calorically imperfect gas effects. The Crocco relation was used to compute the boundary-layer total-temperature distributions, using measured forebody and ramp surface temperatures.

The forward ramp rake is located 6.09 cm outboard of the ramp centerline (see Fig. 3 and Table 2). Streamwise rows of pressure taps are located near the rake spanwise station and on the opposite side at $y = 6.88$ cm. Static-pressure data[2,3] show that the rake is located in a significant cross-stream pressure gradient. The oil-flow photograph of Fig. 4b indicates that the surface flow direction at the rake location is greater than 20 deg outboard. Data obtained with the five-hole probe at the boundary-layer edge for the rake streamwise station indicated a yaw-plane flow angle of approximately 13 deg outboard and the corresponding pitot-pressure error of 1%. A 1% correction (increase) was applied to pitot-pressure data obtained from this forward ramp rake. The aft ramp rake is located near the ramp centerline. The flow at this location is nearly streamwise, and no correction was applied to the rake measurements. Boundary-layer rake data transformed by the Van Driest transformation[11] are plotted in law-of-the-wall coordinates[9] in Fig. 9. Values of skin

Table 3 Preston-tube skin-friction data at baseline test conditions, $x = 19.84$ cm

p_{tj}/p_∞	d, cm	y, cm	du_τ/dv_w	C_f
316	0.157	−1.745	180	0.00130
	0.239	−2.380	272	0.00147
	0.318	−3.015	363	0.00146
307	0.157	−1.745	179	0.00133
	0.239	−2.380	272	0.00144
	0.318	−3.015	362	0.00137

friction used in computing the wall coordinates were obtained by the Clauser chart technique.[12]

A review of hypersonic boundary-layer data[9] showed that for $Re_\theta < 10^4$, experimental heat transfer rates are significantly greater than values predicted by methods that are successful in correlating turbulent-boundary-layer heat transfer data at higher Reynolds numbers. In this Reynolds-number range, exponents obtained from curve fits of experimental velocity-profile data to the equation $u/u_e = (y/\delta)^{1/n}$ are considerably larger ($8 < n < 12$) than the range of 6–7 that is typical of hypersonic turbulent boundary layers at higher Re_θ. The range of Re_θ for the present forebody boundary layers is 3500 to 3700. Values of the exponent n obtained from curve fits to the forebody boundary-layer data were found to be 12–14. Values of the local skin friction coefficient estimated from these data are $0.00127 < C_f < 0.00130$, which are greater than the value 0.0011 predicted by the Van Driest II theory[11]; this result is consistent with the elevated values of heat transfer associated with $Re_\theta < 10^4$. The momentum-integral equation predicts that the value of Re_θ will be less than 10^4 at the beginning of the curved outer surface of the cowl. As a result, the entire turbulent portion of the forebody boundary layer is in the low-Reynolds-number range.

Boundary-layer momentum- and displacement-thickness values obtained from the forward boundary-layer rake on the ramp at the baseline test conditions were compared with two-dimensional boundary-layer computations. This comparison indicated that transition may have occurred in the vicinity of $x = 0$.

Preston-Tube Data

Table 3 presents skin-friction data obtained at the baseline test conditions from the three Preston tubes next to the forward ramp rake (Fig. 3). The tube diameters were selected and the data were reduced following the recommendations of Hopkins and Keener.[13] The smallest tube is the closest to the recommended size of 0.25δ. The values of C_f in Table 3 for each of the Preston tubes are in acceptable agreement. Values of C_f obtained from the Preston tubes differ from those obtained by the rake because the rake is located in a region of cross-stream gradients and three-dimensional flow, and also because the rake is in a region of significantly lower static pressure. If rake pitot-pressure data obtained from the tube near the wall are reduced using the Preston-tube data correlation, the results agree with values of C_f derived by the Clauser method within 3%. Values of C_f obtained from values of Re_θ measured by the rakes and the Van Driest II theory are $0.00156 \leq C_f \leq 0.00193$, somewhat smaller than the values derived by the Clauser method (Table 2).

Concluding Remarks

Data were obtained from an experiment conducted with a generic nozzle–afterbody model in the 3.5-Ft Hypersonic Wind Tunnel of NASA Ames Research Center to characterize experimentally the flowfield created by the interaction of SERN flow with a hypersonic external stream. The model design and test planning were performed in close cooperation with members of the Ames NASP CFD team. This paper presents experimental results consisting of oil-flow and shadowgraph flow-visualization photographs, afterbody surface-pressure distributions, boundary-layer rake measurements, and Preston-tube skin-friction measurements. These data are available from CFD code validation.

Surface oil-flow patterns show where the jet-plume flow is attached to the afterbody surface at jet pressure ratios (ratio of jet total to freestream static pressure) of 150 or more. The oil streaks show the region of large outward turning of the underexpanded jet just downstream of the cowl. The oil flow also shows the pattern of lines where the jet flow separates from the ramp, as a result of interaction of the jet-plume internal shock wave with the ramp boundary layer. The flow is attached to the ramp at the cowl exit station, and the separation lines approach the model centerline near the afterbody trailing edge. Shadowgraph photographs show the flowfield characteristics of the jet plume and the forebody. Features associated with the flow ahead of the jet plume are 1) shock waves from the model leading edge and the boundary-layer trips, 2) a turbulent boundary layer on the forebody, starting ahead of the forebody midsection, and 3) boundary-layer separation forward of the cowl trailing edge. Features associated with the jet plume include 1) the shock wave in the external flow that results from the expansion of the jet, 2) the shear layer between the jet and the external flow, 3) the shock wave within the plume, and 4) the boundary within the plume between two expansion regions: a) the two-dimensional, 20-deg expansion at transition from the nozzle exit to the ramp and b) the outward expansion of the flow from the cowl trailing edge. Boundary-layer rake data indicate that the turbulent portion of the forebody boundary layer is of the low-Reynolds-number type. Ramp rake data indicate that boundary-layer transition may have occurred near the combustor exit station at the baseline test conditions.

Acknowledgments

This research was conducted by the NASA Ames Research Center in cooperation with the McDonnell Douglas Independent Research and Development Program. The test was proposed by Gary Chapman, formerly Staff Scientist for the Thermosciences Division, NASA Ames Research Center; now Adjunct Professor, University of California at Berkeley. One of the authors (Keener) was supported by a grant from NASA to Eloret Institute (NCC2-553). Our thanks also to Bill Lockman, NASA Ames Research Center, Research Scientist and Technical Monitor for the grant; Burt Uebelhoer, Model Design Engineer; Mike Frediani, Senior Model Craftsman; and Mike Reeves, Facility Lead Mechanic, responsible for shadowgraph setup and photographs.

References

[1]Marvin, J. G., "CFD Validation Experiments for Hypersonic Flows," AIAA Paper 92-4024, July 1992.

[2]Spaid, F. W., Keener, E. R., and Hui, F., "Experimental Results for a Hypersonic Nozzle/Afterbody Flow Field," NASA TM 4638, March 1995.

[3]Spaid, F. W., and Keener, E. R., "Hypersonic Nozzle–Afterbody Experiment: Flowfield Surveys," *Journal of Spacecraft and Rockets*, Vol. 33, No. 3, 1996, pp. 333–338.

[4]Ruffin, S. M., Venkatapathy, E., Keener, E. R., and Nagaraj, N., "Computational Design Aspects of a NASP Nozzle–Afterbody Experiment," AIAA Paper 89-0446, Jan. 1989.

[5]Ruffin, S. M., Venkatapathy, E., Keener, E. R., and Spaid, F. W., "Single Expansion Ramp Nozzle Simulations," AIAA Paper 92-0387, Jan. 1992.

[6]Spaid, F. W., and Keener, E. R., "Experimental Results for a Hypersonic Nozzle–Afterbody Flow Field," AIAA Paper 92-3915, July 1992.

[7]Spaid, F. W., and Keener, E. R., "Hypersonic Nozzle–Afterbody CFD Code Validation—Part I: Experimental Measurements," AIAA Paper 93-0607, Jan. 1993.

[8]Hopkins, E. J., Keener, E. R., and Louie, P. T., "Direct Measurements of Turbulent Skin Friction on a Nonadiabatic Flat Plate at Mach Number 6.5 and Comparison with Eight Theories," NASA TN D-5675, Feb. 1970.

[9]Keener, E. R., and Hopkins, E. J., "Turbulent Boundary-Layer Velocity Profiles on a Nonadiabatic Flat Plate at Mach Number 6.5," NASA TN D-6907, Aug. 1972.

[10]*Handbook of Flowmeter Orifice Sizing*, Handbook 10B900, Fischer and Porter.

[11]Van Driest, E. R., "Turbulent Boundary Layer in Compressible Fluids," *IAS Journal*, Vol. 18, No. 3, 1951, pp. 145–160.

[12]Clauser, F. H., "Turbulent Boundary Layers in Adverse Pressure Gradients," *Journal of the Aeronautical Sciences*, Vol. 21, Feb. 1954, pp. 91–108.

[13]Hopkins, E. J., and Keener, E. R., "Study of Surface Pitots for Measuring Turbulent Skin Friction at Supersonic Mach Numbers, Adiabatic Wall," NASA TN D-3478, July 1966.

K. J. Weilmuenster
Associate Editor